

# Micro-mechanic modeling of the stress–strain curves of a TiNiCu shape memory alloy

A.H.Y. Lue<sup>a</sup>, Y. Tomota<sup>b</sup>, M. Taya<sup>a,\*</sup>, K. Inoue<sup>a</sup>, T. Mori<sup>a</sup>

<sup>a</sup> Department of Mechanical Engineering, University of Washington, Seattle, WA 98195-2600, USA

<sup>b</sup> Department of Materials science, Ibaraki, University, Japan

## Abstract

A micro-mechanic model based on Eshelby's method and the minimization of the Gibbs free energy criterion, is proposed and used to predict the orientation angles of martensite variants in a single crystal TiNiCu shape memory alloy, which are in a good agreement with the observations by Saburi et al. Then, the stress–strain curve of a single crystal TiNiCu is predicted and is found to be dependent on the mode of applied stress, i.e. tension and compression. The above model is extended to the case of polycrystal TiNiCu system which is assumed to be composed of finite number of grains with several martensite variants being embedded in each grain. It turns out that use of only small number of grains are needed to simulate the smooth stress–strain curve of TiNiCu system. The stress–strain curves in both loading and unloading modes are correctly predicted at an equilibrium temperature. Finally this polycrystal model is applied for other temperatures, indicating the correct temperature dependance of the stress–strain curves. Published by Elsevier Science S.A.

*Keywords:* Shape memory alloy; Martensite; Austenite; Single crystal; Polycrystal; TiNiCu

## 1. Introduction

Shape memory alloys are becoming increasingly important actuator materials that can exhibit large strains (up to 8–10%) with corresponding large magnitude of stress. Among many shape memory alloys (SMAs), TiNi is the most popular and promising SMA [1] being expected as a smart material [2]. For application of SMAs to mechanical parts or devices of actuators, accurate constitutive equations of a SMA are required. Some attempts have been made by using phenomenological models [3], but a more fundamental approach such as a micromechanic model to bridge the microstructure of a SMA to its constitutive equations is strongly desired. As to the micromechanic modeling, several attempts have been made to bridge crystallographic transformation behavior and an overall stress–strain behavior of a SMA. Ono and Satoh [4] and Ono et al. [5] attempted to describe the flow curves of SMA polycrystals by modifying Taylor model [6], in which they adopted a model proposed by Patel and Cohen [7] to express stress-induced martensitic transformation.

Following their works, Buchheit and Wert [8] and their co-workers [9,10] have proposed a generalized Schmidt's law using 'plane stress transformation surfaces' for NiTi, CuAlNi, and NiAl single crystal SMAs, which are similar to so called 'yielding surface'. On the other hand, Patoor et al. [11,12] and Lexcelent et al. [13] have used micromechanics-based modeling; Lexcelent et al. [13] have proposed a model based on Eshelby inclusion theory [14] to describe transformation behavior of a single crystal CuZnAl. However, their derivation of flow stress from Helmholtz free energy change and related interpretations are puzzling. We believe, a stress–strain curve in a SMA accompanying stress-induced martensitic transformation should be computed based on Gibbs free energy change. In order to connect transformation behavior to thermodynamic data directly, the modeling based on Gibbs free energy change should be used.

In this study, Gibbs free energy change is used for simulating stress–strain curves of a SMA accompanying martensitic transformation in single crystals with various orientations and those in polycrystals. That is, by employing Gibbs free energy minimum criterion, martensite habit planes, choice of martensite variants

\* Corresponding author.

formed under external applied stress, threshold stress for onset of stress-induced martensitic transformation and the entire stress–strain curves including loading and unloading will be systematically studied. The predicted results are compared with the experimental data of TiNiCu SMA for verifying the present model because TiNiCu system involves only the phase transformation between martensite and austenite without other phase transformation, and the crystallographic, thermodynamic and mechanical data for this alloy are available from literature [15–18].

## 2. Single crystal

### 2.1. General formulation

#### 2.1.1. Chemical free energy change for martensitic transformation

First, we consider the case of a SMA without applied stress, where Helmholtz free energy ( $F$ ) is identical with Gibbs free energy.

$$F_A = H_A - TS_A \quad (1a)$$

$$F_M = H_M - TS_M \quad (1b)$$

Here,  $H$  is enthalpy,  $T$ , is absolute temperature, and  $S$  is entropy. The subscripts A and M stand for austenite and martensite, respectively. An energy change form is more appropriate to describe a two-phase system energy for we know only their differences (not absolute values), i.e.

$$\Delta F_{(A \rightarrow M)} = F_M - F_A = (H_M - H_A) - T(S_M - S_A) \quad (2)$$

If  $Q$  is the only heat emitted or absorbed during martensite or austenite transformation, the entropy difference can be expressed as

$$(S_M - S_A) = \frac{Q}{T} \quad (3)$$

Using the data obtained from differential scanning calorimeter (DSC) tests (Fig. 1), the estimation of the equilibrium temperature ( $T_0$ ) [19] and entropy change ( $S_M - S_A$ ) during the martensitic transformation are as follows,

$$T_0 = \frac{A_f + M_s}{2} \quad (4)$$

$$(S_M - S_A) = \frac{Q_{(A \rightarrow M)} + |Q_{(M \rightarrow A)}|}{2T_0} \quad (5)$$

Here,  $M_s$  is the start temperature of martensitic transformation ( $A \rightarrow M$ ) and  $A_f$  is the finish temperature of austenite (or reverse) transformation ( $M \rightarrow A$ ). The relationship between  $\Delta F_{(A \rightarrow M)}$  and temperature ( $T$ ) is schematically drawn in Fig. 1b, where linear approximation is usually made around  $T_0$ .

Experimental results have shown that a thermal martensitic transformation does not occur at  $T_0$  but for below  $T_0$ , instead. Therefore,  $\Delta F_{(A \rightarrow M)}$  is not the only dominant factor for the growth of martensite variants. A resistance (friction energy) must also be considered for the growth of martensite variants. Such a friction energy can be obtained from some experimental work [13,20]. The friction energy can be overcome by either supercooling the system or applying external stresses.

At an arbitrary temperature above  $M_s$ , the sum of  $\Delta F_{(A \rightarrow M)}$  and the friction energy, denoted by  $\Delta G \#$ , must be balanced mechanically for stress-induced martensitic transformation to occur (see gray area in Fig. 1c).  $\Delta G \#$  is a function of temperature and can be obtained as following (refer to Fig. 1 and Section 2.2.2).

Step 1, to obtain transformation temperatures ( $M_s$  and  $A_f$ ) and transformation heat ( $Q$ ) from DSC test.  
Step 2, to obtain  $\Delta F_{(A \rightarrow M)}$  versus  $T$  relationship by estimating  $T_0$  and  $(S_M - S_A)$ .

Step 3, to add friction energy to obtain  $\Delta G \#$ .

$\Delta G \#$  so obtained will be used for the criterion of stress-induced martensite transformation as will be discussed in Section 2.1.2.

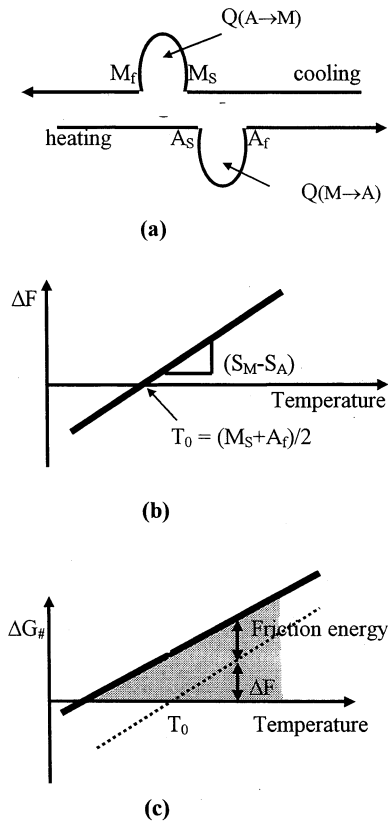


Fig. 1. (a) DSC data to calculate  $T_0$  and slope of  $\Delta F-T$  curve; (b) chemical free energy change  $\Delta F-T$  curve; (c) criterion of martensitic transformation  $\Delta G \# -T$  curve.

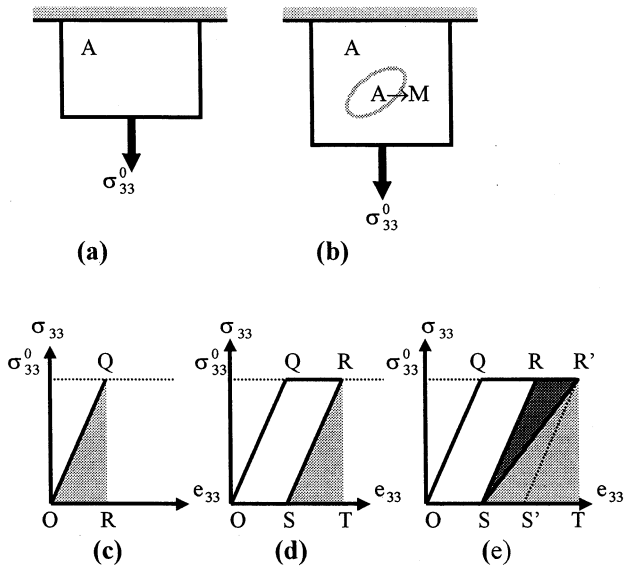


Fig. 2. Uniaxial stress applied to austenite specimen, (a) before transformation; (b) after transformation and stress-strain curve for (c) austenite only; (d) austenite plus a portion of martensite ( $E_A = E_M$ ); (e) austenite plus a portion of martensite ( $E_A \neq E_M$ ).

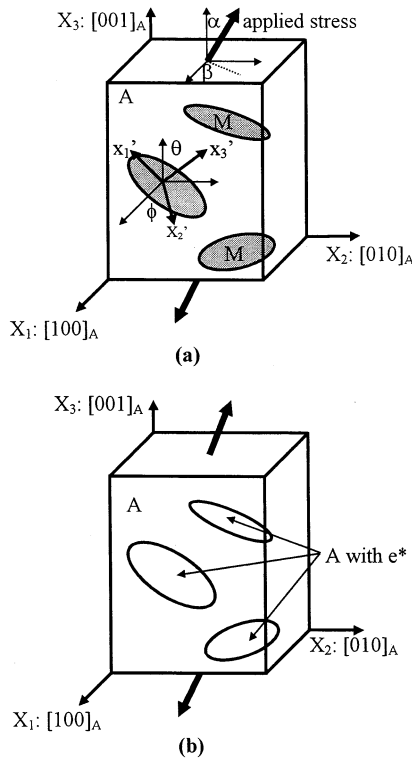


Fig. 3. (a) Stress-induced martensite variants in austenite specimen; (b) inclusions with eigenstrain  $e^*$  in austenite specimen. A, austenite; M, martensite.

2.1.2. Micromechanical modeling for stress-induced martensitic transformation

When an uniaxial external stress is applied to a specimen, Gibbs free energy change ( $\Delta G_{(A \rightarrow M, \sigma^0)}$ ), in-

stead of  $\Delta F_{(A \rightarrow M)}$ , should be used to describe the system free energy. That is, the work done by the applied stress should be added to Eq. (2) to express  $\Delta G_{(A \rightarrow M, \sigma^0)}$ .

Gibbs free energy changes before and after stress-induced martensitic transformation under applied stress may be generally written as,

$$\Delta G_{(A \rightarrow M, \sigma^0)} = \Delta G \# + \Delta W_{\text{surf}} + \Delta G_{\text{mech}} \tag{6}$$

Here,  $\Delta W_{\text{surf}}$  is the interfacial energy, which is usually considered to be negligible in SMAs [13].  $\Delta G_{\text{mech}}$  is mechanical energy due to internal and external stresses. Then, a criterion for the onset of stress-induced martensitic transformation can be defined by:

$$\Delta G \# + \Delta G_{\text{mech}} \leq 0 \tag{7}$$

When the martensite transformation occurs under external stress ( $\sigma_{ij}^0$ ) as shown in Fig. 2,  $\Delta G_{\text{mech}}$  is written as:

$$\begin{aligned} \Delta G_{\text{mech}} = & \left\{ \frac{1}{2} \int_D (\sigma_{ij}^0 + \sigma_{ij}) (u_{i,j}^0 + u_{i,j} - e_{ij}^T) dv \right. \\ & \left. - \int_S F_i (u_i^0 + u_i) ds \right\} \\ & - \left\{ \frac{1}{2} \int_D \sigma_{ij}^0 u_{i,j}^0 dv - \int_S F_i u_i^0 ds \right\} \end{aligned} \tag{8}$$

where  $\sigma_{ij}^0$  is external stress,  $u_{i,j}^0$  is displacement gradient induced by  $\sigma_{ij}^0$ ,  $\sigma_{ij}$  is disturbance stress due to transformation strain  $e_{ij}^T$  and elastic inhomogeneity effect,  $u_{i,j}$  is disturbance displacement gradient corresponding to  $\sigma_{ij}$ ,  $F_i$  is applied force,  $D$  is the specimen volume and  $S$  is the surface of the specimen. In the case of uniaxial external stress, the first  $\{ \}$  term of Eq. (8) is corresponding to Fig. 2b while the second term to Fig. 2a.

Through some mathematical manipulations and using Gauss divergence theorem and equilibrium equation, Eq. (8) is reduced to

$$\begin{aligned} \Delta G_{\text{mech}} = & -\frac{1}{2} \left\{ \int_{\Omega} \sigma_{ij}^0 e_{ij}^* dv + \int_{\Omega} \sigma_{ij}^0 e_{ij}^T dv + \int_{\Omega} \sigma_{ij} e_{ij}^T dv \right\} \\ = & A + B + C \end{aligned} \tag{9}$$

where  $\Omega$  is the volume of martensite variants,  $e_{ij}^*$  is equivalent eigenstrain to be solved.

To solve  $e_{ij}^*$ , we use a micromechanic model (Fig. 3a) in which martensite variants with  $e_{ij}^T$  are approximated by prolate ellipsoids expressed by,

$$\frac{x_1'^2}{a^2} + \frac{x_2'^2}{b^2} + \frac{x_3'^2}{c^2} = 1 \tag{10}$$

where ‘prime’ denotes the local coordinates attached to each martensite variant, all martensite variants are assumed to be penny-shaped, i.e.  $a = b$ . The problem of Fig. 3a is then converted to that of Fig. 3b by using Eshelby equivalent inclusion theory [14,21];

$$\sigma_{ij}^0 + \sigma'_{ij} = C_{ijk}^M (e_{kl}' + \bar{e}'_{kl} + e'_{kl} - e_{kl}^T)$$

$$= C_{ijkl}^A (e_{kl}^{0'} + \bar{e}'_{kl} + e'_{kl} - e_{kl}^{*'}) \quad (11)$$

where  $C_{ijkl}^M$  and  $C_{ijkl}^A$  refer to the elastic moduli of martensite and austenite, respectively.  $E_{kl}^0$  is the uniform strain, which is related to the applied stress  $\sigma_{ij}^{0'}$  by

$$\sigma_{ij}^{0'} = C_{ijkl}^A e_{kl}^{0'}, \quad (12)$$

$e'_{kl}$  is the disturbance strain related to the equivalent eigenstrain ( $e_{mn}^{*'}$ ) through the Eshelby's tensor as

$$e'_{kl} = S_{klmn} e_{mn}^{*'} \quad (13)$$

Following Mori–Tanaka mean field concept [22], the average disturbance strain ( $\bar{e}'_{kl}$ ) is given by

$$\bar{e}'_{kl} = -\sum_I^N f_I T_I \{e'_{kl}(I) - e_{kl}^{*'}(I)\} \quad (14)$$

where  $f_I$  is the volume fraction of the  $I$ th martensite variant,  $N$  is the total number of variants, and  $T_I$  is a coordinate transformation matrix from the local coordinates attached to each martensite to the global coordinates attached to the austenite or specimen. Then, the averaged strain in the local coordinates ( $\bar{e}'_{kl}$ ) is related to that in the global by

$$\bar{e}'_{kl} = T_I^{-1} \bar{e}_{kl} \quad (15)$$

where

$$T_I = \begin{bmatrix} c^2\theta c^2\phi & s^2\phi & s^2\theta c^2\phi & -2s\theta s\phi c\phi & 2s\theta c\theta c^2\phi & -2c\theta s\phi c\phi \\ c^2\theta s^2\phi & c^2\phi & s^2\theta s^2\phi & 2s\theta s\phi c\phi & 2s\theta c\theta s^2\phi & 2c\theta s\phi c\phi \\ s^2\theta & 0 & c^2\theta & 0 & -2s\theta c\theta & 0 \\ -s\theta c\theta s\phi & 0 & s\theta c\theta s\phi & c\theta c\phi & s\phi(c^2\theta - s^2\theta) & -s\theta c\phi \\ -s\theta c\theta c\phi & 0 & s\theta c\theta c\phi & -c\theta s\phi & c\phi(c^2\theta - s^2\theta) & s\theta s\phi \\ c^2\theta s\phi c\phi & -s\phi c\phi & s^2\theta s\phi c\phi & s\theta(c^2\phi - s^2\phi) & 2s\theta c\theta s\phi c\phi & c\theta(c^2\phi - s^2\phi) \end{bmatrix} \quad (16)$$

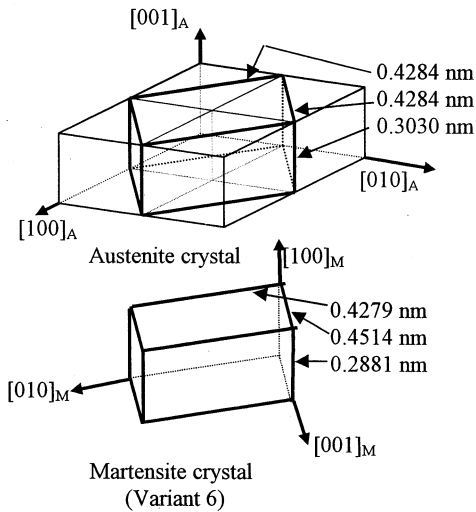


Fig. 4. Lattice distance of austenite and martensite of a Ti–40at.%Ni–10at.%Cu sample.

and where  $s\theta = \sin \theta$ ,  $s\phi = \sin \phi$ ,  $c\theta = \cos \theta$ ,  $c\phi = \cos \phi$ .

Using Eqs. (11)–(13), (15) and (16),  $e_{kl}^{*'}$  and  $\sigma_{ij}$  can be obtained.

## 2.2. Input data for computations

### 2.2.1. Transformation strains

In this paper, a Ti–40at.%Ni–10at.%Cu SMA sample is chosen. The sample's parent phase (austenite) with B2 structure transforms to the martensite phase with orthorhombic structure, as shown in Fig. 4. The changes in the lattice parameters are 0.3030 nm → 0.2881 nm in [100], 0.4284 nm → 0.4279 nm in [010], and 0.4284 nm → 0.4284 nm in [001] upon martensite transformation [15]. Both on these data  $e_{ij}^{T'}$  is calculated in the martensite (local) coordinate:

$$e_{ij}^{T'} = \begin{bmatrix} -0.0492 & 0 & 0 \\ 0 & -0.0012 & 0 \\ 0 & 0 & 0.0537 \end{bmatrix} \quad (17)$$

The phenomenological study for this alloy indicates that lattice invariant shear is not needed [15]. Table 1

shows the corresponding orientations between six variants possibly formed in this alloy and the austenite. Six transformation strains ( $e_{ij}^{T'}$ ) described in the austenite (global coordinates) are

Table 1  
Comparison between predicted and observed orientations of habit planes of six variants

Variant	$\theta$ (pred.)	$\theta$ (obsv.)	$\phi$ (pred.)	$\phi$ (obsv.)
V1	60	59	–36/–144	–37/–143
V2	60	59	36/–144	37/–143
V3	60	59	126/–126	127/–127
V4	60	59	54/–54	53/–53
V5	46	47	135/–45	135/–45
V6	46	47	45/–135	45/–135

$$e_{ij}^T = \begin{bmatrix} -p & 0 & 0 \\ 0 & q & -r \\ 0 & -r & q \end{bmatrix}, \begin{bmatrix} -p & 0 & 0 \\ 0 & q & r \\ 0 & r & q \end{bmatrix}, \begin{bmatrix} q & 0 & -r \\ 0 & -p & 0 \\ -r & 0 & q \end{bmatrix}, \begin{bmatrix} q & 0 & r \\ 0 & -p & 0 \\ r & 0 & q \end{bmatrix}, \begin{bmatrix} q & -r & 0 \\ -r & q & 0 \\ 0 & 0 & -p \end{bmatrix}, \begin{bmatrix} q & r & 0 \\ r & q & 0 \\ 0 & 0 & -p \end{bmatrix}, \quad (18)$$

respectively, where  $p = 0.0492$ ,  $q = 0.0263$  and  $r = 0.0275$ .

In this study, the Young's moduli and Poisson's ratios of the austenite and martensite are, respectively, taken to be 67.0 GPa and 0.43 and 26.3 GPa and 0.43.

### 2.2.2. Temperature dependence of free energy

$\Delta G \#$  in Eq. (7) is estimated from the DSC data,  $M_s = 345$  K,  $A_f = 378$  K and  $Q = 400$  cal mol<sup>-1</sup> ( $= 237$  MJm<sup>-3</sup>) [16]. Thus,  $T_0$  (Eq. (4)) becomes 361 K. Free energy curves in Fig. 1b is then described as,

$$\Delta F = 0.657(T-361) \text{ MJm}^{-3} \quad (19)$$

Some experiment is needed to determine precise friction energy as described in Section 2.1.1. However, here, for simplicity, neglecting its temperature dependence, the friction energy ( $G_f$ ) is estimated from energy change ( $\Delta F$ ) at  $M_s$  by  $G_f = 10$  MJm<sup>-3</sup>. Then, adding  $G_f$  to  $\Delta G \#$  given by

$$\Delta G \# = 0.657(T-345) \text{ MJm}^{-3} \quad (20)$$

## 2.3. Results and discussions

### 2.3.1. Habit plane

First, we calculated  $\Delta G_{\text{mech}}$  and then minimized it with respect to spherical orientation angles ( $\theta$ ,  $\phi$ ) and aspect ratio of martensite variant, i.e.  $c/a$  in Eq. (10) with and without applied stress at various volume fractions of  $i$ th martensite variant ( $f_i$ ), i.e.

$$\frac{\partial \Delta G_{\text{mech}}}{\partial \theta_i} = 0 \quad (21a)$$

$$\frac{\partial \Delta G_{\text{mech}}}{\partial \phi_i} = 0 \quad (21b)$$

It is found that the values of  $\theta$  and  $\phi$  are almost independent of  $f_i$  and applied stress. Habit planes are experimentally defined from a very early stage of martensite variant formation [15] and are not considered to differ by changing  $f_i$  or applying external stress. Following the experiment by Saburi et al. [15], we set

$f_i = 0.001$  (0.1%) and obtained the minimum  $\Delta G_{\text{mech}}$  at  $c/a \rightarrow 0$ ,  $\theta = 46$  and  $\phi = 45$  or  $-135$  for variant V6. Saburi et al. [15] have reported that very thin plate martensite with the habit plane between  $\{334\}$  ( $\theta = 47$  for V6) and  $\{223\}$  ( $\theta = 43$ ) is observed in the TiNiCu SMA. Therefore, the present predictions are very close to the observations. Such minimization conditions are applied for other variants only by consideration of geometrical rotation.

Next, we shall take a reasonable approximation for  $e_{ij}^T$  so that more clear understanding of the martensite transformation can be obtained. By ignoring  $e_{22}^T$  component in Eq. (17) due to its smallness  $e_{ij}^T$  can be approximated as

$$e_{ij}^{T'} = \begin{bmatrix} -0.0492 & 0 & 0 \\ 0 & 0 & 0 \\ 0 & 0 & 0.0537 \end{bmatrix} \quad (22)$$

If a martensite variant with  $c/a \rightarrow 0$  and  $\varepsilon_{22}^{T'} = 0$  is rotated by an angle  $\theta'$  around the  $x'_2$  axis (martensite coordinates),  $e_{ij}^{T'}$  is transformed to  $e_{ij}^{T''}$  expressed in double prime coordinate as:

$$e_{ij}^{T''} = \begin{bmatrix} \varepsilon_{11}^{T'} \cos^2 \theta' + \varepsilon_{33}^{T'} \sin^2 \theta' & 0 & (\varepsilon_{33}^{T'} - \varepsilon_{11}^{T'}) \sin \theta' \cos \theta' \\ 0 & 0 & 0 \\ (\varepsilon_{33}^{T'} - \varepsilon_{11}^{T'}) \sin \theta' \cos \theta' & 0 & \varepsilon_{11}^{T'} \sin^2 \theta' + \varepsilon_{33}^{T'} \cos^2 \theta' \end{bmatrix} \quad (23)$$

When,  $\varepsilon_{11}^{T''} = \varepsilon_{11}^{T'} \cos^2 \theta' + \varepsilon_{33}^{T'} \sin^2 \theta' = 0$  is imposed, i.e.

$$2\theta' = \cos^{-1} \left\{ \frac{(\varepsilon_{33}^{T'} + \varepsilon_{11}^{T'})}{(\varepsilon_{33}^{T'} - \varepsilon_{11}^{T'})} \right\} \quad \text{or} \quad \theta = \tan^{-1} \left( -\frac{\varepsilon_{11}^{T'}}{\varepsilon_{33}^{T'}} \right) \quad (24)$$

there is no elastic interaction between the martensite variant and the matrix, i.e. elastic strain energy is zero as shown in Appendix A. Therefore, the strain energy of a SMA containing such martensite transformation strain becomes zero by taking extreme variant shape ( $c/a \rightarrow 0$ ) and the habit plane orientation ( $\theta'$ ) defined by Eq. (24). Substituting Eq. (22) into Eq. (24), we obtain  $\theta' = \pm 43.8$ . Converting  $\theta'$  to the austenite (global) coordinates under the lattice correspondence (Table 1), we obtain  $\theta = 46$ ,  $\phi = 45$  or  $-135$  for V6 which are in good agreements with the observations [15].

Elastic strain energy of inclusions with various shapes and various eigenstrains have been studied so far [23–26]. In such studies, one inclusion is embedded in the infinite matrix. Effects of shape, types of eigenstrains and elastic moduli difference have been made

Table 2

Example calculation of Eq. (9) for V2.  $E_A = 67$  GPa,  $E_M = 26.3$  GPa,  $\sigma_{33}^0 = 187$  MPa,  $[hkl] = [011]$ , and volume fraction  $f_2 = 0.1$  (unit:  $10^{-5}$  GJ/m<sup>3</sup>)

	A	B	C
$E_A = E_M$	-37.66	-37.66	0.02
$E_A \neq E_M$	-40.16	-37.66	-3.15

clear. In the case of penny-shaped plate inclusion ( $a = b, c/a \rightarrow 0$ ) with transformation strains of  $\epsilon_{11}^T < -v\epsilon_{22}^T < \epsilon_{33}^T$ , the elastic strain energy ( $W$ ) becomes minimum when the normal direction of the plate, i.e. habit plane, is given by

$$\left[ \frac{- (\epsilon_{11}^T + v\epsilon_{22}^T)}{(\epsilon_{33}^T - \epsilon_{11}^T)} \right]^{1/2}, 0, \left[ \frac{(\epsilon_{33}^T + v\epsilon_{22}^T)}{(\epsilon_{33}^T - \epsilon_{11}^T)} \right]^{1/2} \quad (25)$$

Then, at  $\theta' = \tan^{-1}(-\epsilon_{11}^T/\epsilon_{33}^T)$ , the minimum elastic strain energy becomes a function of only  $\epsilon_{22}^T$  and elastic moduli of the inclusion, i.e.

$$W = \{\mu(1 + \nu)\}(\epsilon_{22}^T)^2 \quad (26)$$

Therefore,  $W$  becomes zero if  $\epsilon_{22}^T = 0$ . The results are consistent with the above simple discussion.

Hereafter, we adopt  $\theta = 46, \phi = 45$  or  $-135$  and  $c/a \rightarrow 0$  for variant V6 in the following computations. The angles and  $c/a$  for other variants are also set similarly by geometrical rotation.

2.3.2. Variant choice under applied stress

When elastic moduli of austenite and martensite are assumed to be identical ( $C_{ijkl}^A = C_{ijkl}^M, E = 67$  GPa),  $e_{ij}^*$  is equal to  $e_{ij}^T$ . The sum of (A + B) in Eq. (9) becomes  $-\int_{\Omega} \sigma_{ij}^0 e_{ij}^T dv$  which is the potential change ( $V$ ) corresponding to an area OQRS in Fig. 2d. The term  $C$  in Eq. (9) is found to be almost zero. Examples of calculated A, B and C terms are shown in Table 2. As we have found in the previous section that the elastic strain energy of the present martensite variant embedded in the infinite matrix is zero, then, the interaction energy among various variant is also zero. As a result,  $\Delta G_{mech}$  is found to be equal to the potential change. Therefore, the energy which we should calculate for Gibbs free energy change under the applied stress becomes only  $-\sigma_{33}^0 \epsilon_{33}^T$ , where  $\sigma_{33}^0$  and  $\epsilon_{33}^T$  refer to the applied stress and transformation strain along  $[hkl]$  in the austenite coordinates.

Table 3

Calculated transformation strain  $\epsilon_{33}^T[hkl]$  in austenite coordinates  $[hkl]$  (T: variant appears in tension; C: variant appears in compression)

$[hkl]$	v1	v2	v3	v4	v5	v6
[001]	+0.0269 T	+0.0269 T	+0.0269 T	+0.0269 T	-0.0492 C	-0.0492 C
[011]	+0.0000	+0.0537 T	-0.0112 C	-0.0112 C	-0.0112 C	-0.0112 C
$[\bar{1}11]$	-0.0164 C	+0.0195 T	+0.0195 T	-0.0164 C	+0.0195 T	-0.0164 C
$[\bar{1}23]$	-0.0016	+0.0445 T	+0.0164	-0.0064	-0.0143	-0.0297 C

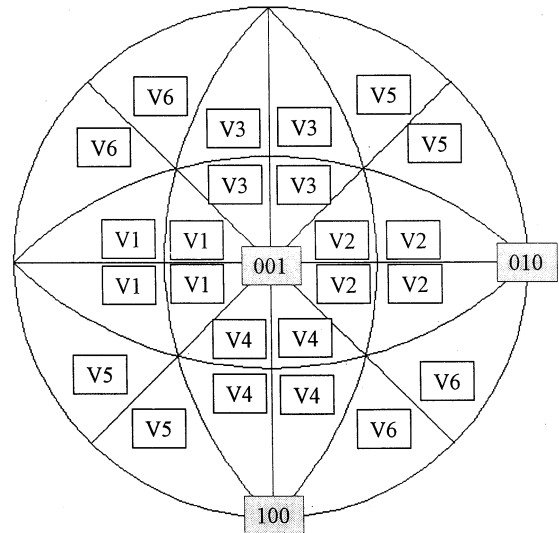


Fig. 5. Martensite variant choice for a given tension in specified direction (stereographic plotting).

The transformation strains for six variants along  $[hkl]$  ( $\epsilon_{33}^T[hkl]$ ) can be evaluated simply by

$$\epsilon_{33}^T(I)[hkl] = \left\{ \frac{1}{(h^2 + k^2 + l^2)} \right\} [h, k, l]^t e_{ij}^T(I) [h, k, l] \quad (27)$$

Then, the variant with the largest  $\epsilon_{33}^T[hkl]$  is expected to give the lowest Gibbs free energy change. Table 3 lists variant's  $\epsilon_{33}^T[hkl]$  in [001], [011], [111], and [123]. The preferred variant choice for a given tensile stress in the specified direction (based on the austenite coordinates) are calculated and summarized in Fig. 5.

When Young's moduli are different ( $E_A \neq E_M$  or equivalently  $C_{ijkl}^A \neq C_{ijkl}^M$ ), elastic inhomogeneity effect must be taken into consideration. As shown in Fig. 2b, the average stiffness of a specimen ( $E_S$ ) changes with increasing martensite volume fraction. The equivalent eigenstrain ( $e_{ij}^*(I)$ ) should be used instead of  $e_{ij}^T(I)$ . As a result, the Gibbs free energy change is decreased by an area  $\Delta SRR'$  in Fig. 2e. This is analogical to the case of Griffith crack growth [27]. It can be summarized that stress induced transformation is enhanced when  $E_A \geq E_M$  but suppressed when  $E_A \leq E_M$ . However, as seen in Table 2, the term  $C$  is found much smaller than (A + B) in Eq. (9), so that the influence of elastic inhomogeneity effect on variant choice under applied stress can be neglected in the TiNiCu SMA.

### 2.3.3. Stress–strain curves accompanying stress-induced martensitic transformation

In the case of  $C_{ijkl}^A = C_{ijkl}^M$ , mechanical energy change  $\Delta G_{\text{mech}}$  can be evaluated by only potential energy change,  $V$ , as discussed above,

$$\Delta G_{\text{mech}} = V = -\sigma_{33}^0 \varepsilon_{33}^T [hkl] \quad (28)$$

From Eq. (7), i.e.  $\Delta G_{\text{mech}} = -\Delta G \#$ , and Eq. (28),  $\sigma_{33}^0$  can be found from

$$\sigma_{33}^0 [hkl] = \frac{\Delta G \#}{\varepsilon_{33}^T [hkl]} \quad (29)$$

The predicted flow stresses are illustrated in Fig. 6. They are found to be direction dependent, i.e. tension or compression along  $[hkl]$ .

The onset stress of stress-induced martensite transformation ( $\sigma_M$ ) can be roughly discussed from the values of  $\varepsilon_{33}^T [hkl]$  in Table 3. For example, the lowest yield strength of V2 under tension is in  $[011]$  direction followed by  $[123]$ ,  $[001]$ , and  $[111]$  for their  $\varepsilon_{33}^T [hkl]$  are in the reverse order. On the other hand, the lowest  $\sigma_M$  of V6 under compression is in  $[001]$  direction followed by  $[123]$ ,  $[111]$  and  $[011]$ . These predictions are qualitatively in good agreements with the experimental results [17].

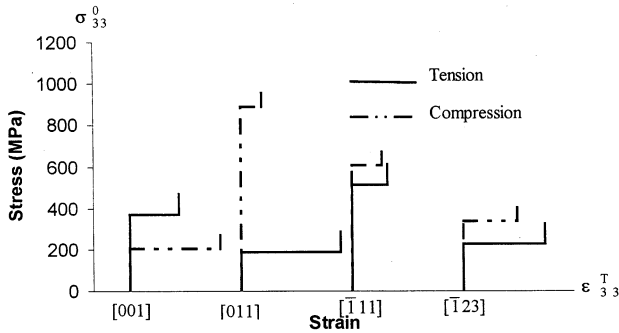


Fig. 6. Predicted flow stresses for the stresses applied in the direction of  $[001]$ ,  $[011]$ ,  $[111]$ , and  $[123]$ .

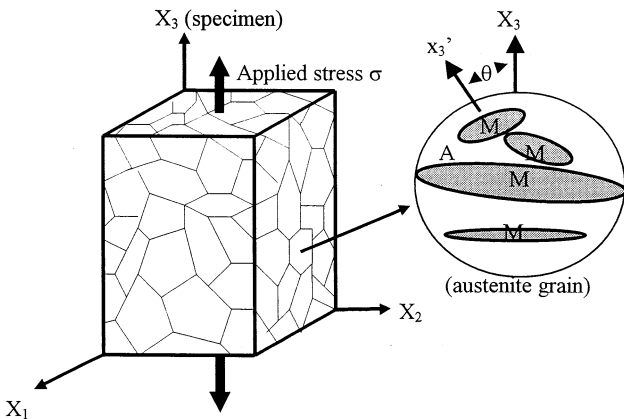


Fig. 7. Polycrystal model. Spherical austenite grains are assumed.

In Fig. 6, the flow curves are drawn up to the fully martensitic transformation. However, the following three points are worth mentioning when compared with real deformation. The first is the assumption of variant shape ( $c/a \rightarrow 0$ ). During transformation,  $c/a$  increases with  $f$ . The internal strain energy corresponding to the term  $C$  of Eq. (9) becomes larger and is no longer negligible. Such an increase in the internal strain energy gives rise to work hardening. This is true with a real SMA as the experimental flow curves usually exhibit some positive slope unlike those seen in this study. This crystal rotation is considered to contribute work hardening, too. The third point is the assumption of  $C_{ijkl}^A = C_{ijkl}^M$ . It is discussed as the following.

If we approximate the elastic energy due to the transformation to be vanishingly small. Thus, the mechanical energy change  $\Delta G_{\text{mech}}$  due to the transformation is roughly calculated as

$$\Delta G_{\text{mech}} = -\sigma_{ij}^0 \varepsilon_{ij}^T - \frac{1}{2} \sigma_{ij}^0 \left( \frac{\sigma_{ij}^0}{E_M} - \frac{\sigma_{ij}^0}{E_A} \right) \quad (30)$$

per unit volume transformed. As will be seen in Fig. 9,  $\varepsilon_{ij}^T$  is in the order of 0.04,  $\sigma_{ij}^0$  in the order of 0.25 GPa,  $E_M = 26.3$  GPa and  $E_A = 67$  GPa. Thus, the second term in Eq. (30) is less than 10% of the first term in Eq. (30). That is, the inhomogeneity effect on the energy can be ignored for all practical purposes, when the mechanical effect on the transformation is examined.

## 3. Polycrystal

### 3.1. Model

In chapter 2, the internal stress within a martensite plate can be approximated to be zero in a single crystal, so that neither the elastic strain energy due to transformation strain nor the interaction of internal stresses among many martensite plates need to be considered. On the other hand, a polycrystal contains variously oriented austenite grains with different stress-induced martensites. The different transformation strains within austenite grains result in misfit strains among the grains.

In order to compute a flow (or stress–strain) curve of a polycrystal TiNiCu, a model shown in Fig. 7 is employed, where an austenite grain is approximated by a sphere. The transformation strain of  $I$ th variant ( $I = 1, 6$ ) in  $J$ th grain,  $\varepsilon_{ij}^T(J, I)$ , can be calculated by using transformation strain listed in Eq. (22) if its orientation relationships with respect to austenite (grain) coordinates as well as specimen coordinates are given. The grains with the same orientation angle  $\theta$  and various  $\phi$ s (refer to Fig. 3) can be converted to a single group of grain with  $\theta$ , i.e. independent of  $\phi$ . Therefore, the transformation strain for the  $I$ th variant in the  $J$ th

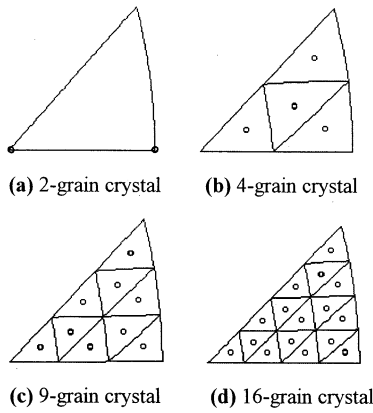


Fig. 8. Mesh in standard stereographic triangle. The centers of smaller triangles are shown by the circles.

grain must be averaged with respect to this rotation ( $\phi$ ). For instance, the averaged transformation strain of variant V2 in the  $J$ th grain loaded in the [011] tensile direction can be written as follows.

$$\varepsilon_{ij}^T(J,2) = \begin{bmatrix} -0.0246 & 0 & 0 \\ 0 & -0.0246 & 0 \\ 0 & 0 & 0.0537 \end{bmatrix} \quad (31)$$

$\varepsilon_{ij}^T(J, I)$  is expressed by such a diagonal matrix for any  $[hkl]$ . Then, the average transformation strain of the  $J$ th grain,  $\varepsilon_{Gij}^T(J)$ , is written as

$$\varepsilon_{Gij}^T(J) = \sum_I^6 f_I(J) \varepsilon_{ij}^T(J, I) \quad (32)$$

where  $f_I(J)$  refers to the unknown volume fraction of the  $I$ th variant in the  $J$ th grain.

The averaged transformation strain in the specimen ( $\varepsilon_{Sij}^T$ ) is the sum of  $\varepsilon_{Gij}^T(J)$  of all grains, i.e.

$$\varepsilon_{Sij}^T = \sum_J^N F_J \varepsilon_{Gij}^T(J) \quad (33)$$

where  $N$  is the total number of austenite grains in a specimen.  $F_J$  is the grain volume fraction of the  $J$ th grain group. Then eigenstrain for the  $J$ th grain is given by

$$\varepsilon_{Gij}^*(J) = \varepsilon_{Gij}^T(J) - \varepsilon_{Sij}^T \quad (34)$$

The internal stress within the  $J$ th grain is computed by Eshelby's method [14] by

$$\sigma_{ij}(J) = \mathbf{C}(\mathbf{S} \cdot \mathbf{I}) \{ \varepsilon_{Gij}^T(J) - \varepsilon_{Sij}^T \} \quad (35)$$

If we take  $E_A \neq E_M$  into account, the elastic moduli of not only each grain but also overall specimen have to be computed step by step with transformation. This is extremely troublesome. Therefore, to simplify the computation, the difference in elastic moduli between austenite and martensite is neglected as discussed in chapter 2.

Thus, the elastic strain energy per unit volume ( $W$ ) is given by:

$$\begin{aligned} W &= -\frac{1}{2} \sum_J^N F_J \sigma_{ij}(J) \varepsilon_{Gij}^T(J) \\ &= -\frac{1}{2} \sum_J^N F_J \sigma_{ij}(J) \sum_I^6 f_I(J) \varepsilon_{ij}^T(J, I) \end{aligned} \quad (36)$$

The potential energy change is expressed by

$$\begin{aligned} V &= -\sum_J^N F_J \sigma_{ij}^0(J) \varepsilon_{Gij}^T(J) \\ &= -\sum_J^N F_J \sigma_{ij}^0(J) \sum_I^6 F_I(J) \varepsilon_{Gij}^T(J, I) \end{aligned} \quad (37)$$

Mechanical energy change for a polycrystal specimen is described by

$$\Delta G_{\text{mech}} = W + V \quad (38)$$

Here,  $\Delta G_{\text{mech}}$  is a function of only unknown  $f_I(J)$  for a given  $\sigma_{ij}^0$ . In the computation,  $\sigma_{ij}^0$  is increased incrementally and for each incremental applied stress  $f_I(J)$  should be solved to minimize the  $\Delta G_{\text{mech}}$  of specimen (Eq. (38)) and satisfy the transformation criterion of variants (Eq. (28)). The potential energy of the  $I$ th variant in the  $J$ th grain is  $(\sigma_{ij}^0 + \sigma_{ij}(J)) \varepsilon_{ij}^T(J, I)$ . Therefore, the criterion for martensite transformation becomes:

$$\{ (\sigma_{ij}^0 + \sigma_{ij}(J)) \varepsilon_{ij}^T(J, I) \} + \Delta G \neq \leq 0 \quad (39)$$

In the case of uniaxial loading the total strain of the specimen is given by:

$$\varepsilon_{S33} = \frac{\sigma_{33}^0}{E_A} + \varepsilon_{S33}^T \quad (40)$$

## 3.2. Result of calculations and discussion

### 3.2.1. Stress-strain curve under applied tensile stress

For examining the case of three-dimensional random distribution of grain orientation, the representative  $[hkl]$ s as shown in Fig. 8 is considered. That is, the standard [001]–[011]–[111] triangle is divided into 4, 9, or 16 regions with approximately the same area on the surface of original crystallographic globe (before stereographic projection) and  $[hkl]$  is determined as the center of each region.

The onset of stress-induced martensite transformation is determined by the start of transformation in a variant with the largest  $\varepsilon_{33}^T(J, I)$ . The  $\Delta G_{\text{mech}}$  of the overall specimen with such a transformation strain becomes the minimum under the applied stress. With increasing  $f_I(J)$ ,  $\sigma_{ij}(J)$  is generated so as to suppress the transformation in the grain, and thus  $\sigma_{ij}^0$  has to be increased for further transformation. At the same time, such internal stress promotes the transformation of other variable in other grains. Therefore, we check Eq. (39) for all variants in all grains, seeking the optimum

volume fractions of  $f_I(J)$  for minimizing  $\Delta G_{\text{mech}}$  of Eq. (38).

As shown in Fig. 9, the results of such calculation for the nine-grain model (Fig. 8) show a flow curve of a polycrystal specimen, which can be divided, into five stages:

Stage 1, elastic deformation of austenite.

Stage 2, martensite transformation occurs in some grains in the specimen while the other grains still experience the elastic deformation of austenite phase.

Stage 3, martensitic transformation occurs in all grains, so that the microstructure is a mixture of austenite and martensite in all grains.

Stage 4, some grains are now fully martensite, then deform only elastically, while stress-induced martensitic transformation continues to occur in the other grains.

Stage 5, martensite transformation is completed in all grains then only the elastic deformation of martensite is observed.

Stage 1 of the curve behaves like any homogeneous elastic material. In stage 2, some grains undergo more transformation than other grains. In fact, the transformation strain along the tensile direction varied from 0 to 0.037, depending on the orientations of the grains, at the end of stage 2. Thus, the internal stresses are accumulated, as stage 2 progresses.

Eventually, the sum of the external and internal stresses results in the same amount of the energy change of the occurrence of the transformation of the most favored variant in all the grains. This is the end of stage 2 and the onset of stage 3.

Because of the criterion adopted in this study, Eq. (7), only a single variant is present in every grain (examined in Fig. 8b–d and Fig. 9). Of course, this is also caused by the present meshing method: a grain is assigned the orientation in the center of a mesh, as shown in Fig. 8b–d. Thus except for the case of Fig. 8a, no grain has a crystallographically highly symmetrical orientation.

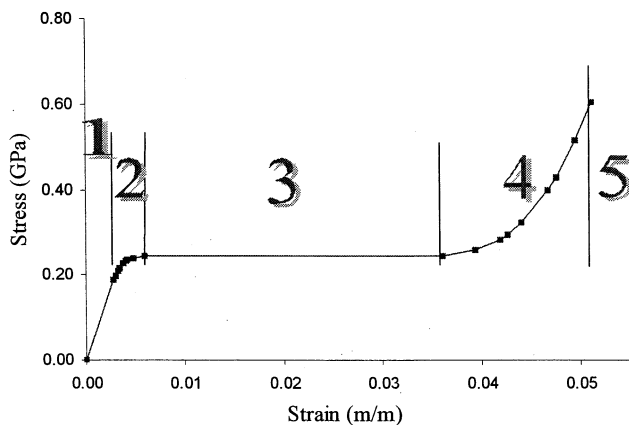


Fig. 9. Tension stress–strain curve of TiNiCu polycrystal.

As seen in Fig. 9, stage 3 covers the widest range of strain and has an almost constant stress. That is, it has extremely small strain hardening. The state of no strain hardening or, equivalently, no additional accumulation of the internal stresses is achieved when all grains have the same plastic strains (produced by the transformation), see Eqs. (34) and (35). This point is checked numerically. The incremental strains are 0.030 along the tensile direction and  $-0.013$  to  $-0.014$  along the transverse directions in all the grains.

The above discussion on what end stage 2 and occurs in stage 3 also indicates the reason for the end of stage 3. At the end, the grains of one particular orientation, grain 9 in Fig. 8, are all covered by a single martensite variant. To continue further transformation, possible only in the other grains, the external stress must be raised at the end of stage 3 and the onset of stage 4. Since at least one group of grains, already covered by the martensite, can deform only elastically, the internal stress is always accumulated after stage 3. Because some other grains gradually become fully covered by the martensite during stage 4, an accelerated increase in the external stress is required in stage 4.

The numerical calculation has also shown that grain 5 starts to transform at the onset of stage 2. As seen in Fig. 6, the [011]-oriented grains have the lowest external stress to induce the transformation in tension. Thus, it is natural that grain 5, near [011], is the first grain to start the transformation. However, the internal stresses caused by the differences in the amount of transformation and the crystallographic orientation between the grains plays an observable role later. For example, at the end of stage 3, grain 9 is all covered by the martensite, while the others are not. The calculation has also indicated that grain 9 has no martensite at the end of stage 2.

Next, we examined the effect of the grain number (Fig. 8) on the shape of stress–strain curve. As shown in Fig. 10, the onset stress of martensitic transformation ( $\sigma_M$ ) is reduced to that of [011] single crystal and the length of stage 3 is decreased with the increase of the grain number. It can be concluded from Fig. 10 that the convergence of the stress–strain curve is rapid as the number of grains increases, indicating that use of not so large number of grains may be adequate in the present model. The stress–strain curve predicted by the present model shows the same shape as that observed by Strnadel et al. [18]. The total transformation strain, i.e. recoverable strain of approximately 4% is in a good agreement with their measured strains. They have also reported that  $\sigma_M$  is proportional to a temperature difference,  $(T - M_s)$ , exhibiting Clausius–Clapeyron relationship. This is easily predictable by the present method from Eq. (20) which shows the linear relationship between  $\Delta G^\#$  and  $(T - M_s)$ .

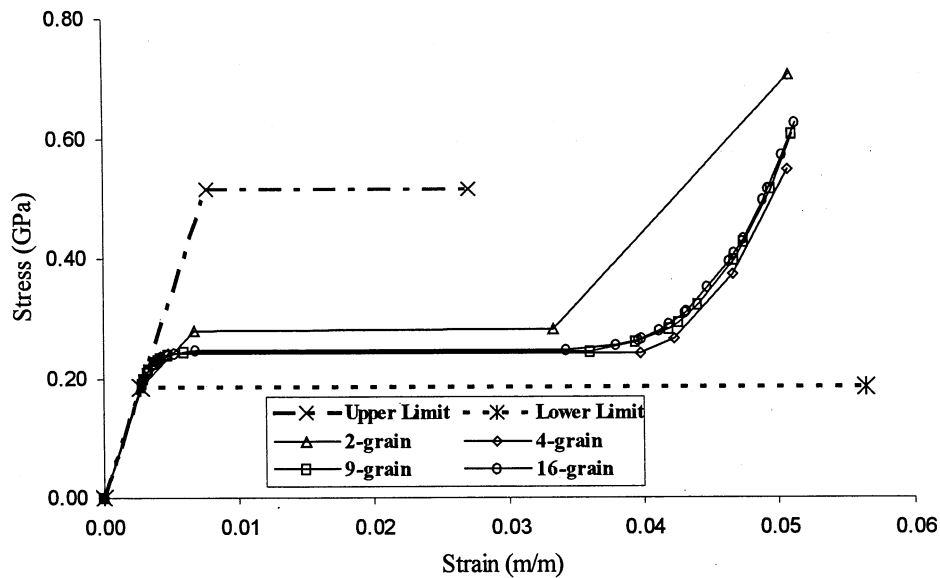


Fig. 10. Tension stress–strain curve of SMA polycrystal.

As can be understood from Fig. 6, the upper limit for the flow stress is given by that of  $[\bar{1}11]$  single crystal, while the lower flow is limited by that of  $[011]$ . These flow curves relevant to  $[\bar{1}11]$  and  $[011]$  single crystal specimens are also shown by dashed lines in Fig. 10. If we have information about the texture of a polycrystal specimen, its flow curve can easily be computed by the present method by introducing the distribution weight for  $F_i$ . For instance, the flow curve of a specimen showing a texture with  $[011]$  along tensile direction must locate near the lower limit in Fig. 10. The higher flow stress in two-grain model (Fig. 10) is an example of a specimen with a texture of  $\{011\}$  and  $\{0\bar{1}1\}$ .

### 3.2.2. Stress–strain curve under loading and unloading tensile stress

From the discussion given in Section 2.1.1, we have examined that a kind of friction stress hinders the martensitic transformation. Similarly, in the case of reverse-transformation (martensite to austenite), there also exists a friction stress which is against the reverse transformation. At the same temperature, due to the nature of the transformations, these friction stresses should be the same in magnitude while opposite in direction.

In this study, Eq. (7) has been used as a criterion for transformation to occur. Where  $\Delta G \#$  is the sum of the chemical free energy change and the friction energy. For stress-induced martensitic transformation, the onset applied stress is needed to overcome the chemical free energy difference and the friction energy. At a constant temperature, if we reduce the applied stress (unloading) during the martensitic transformation, the direction of the friction stress is reverse, resulting in a

smaller  $\Delta G \#$ . Therefore, a smaller applied stress can provide enough  $\Delta G_{\text{mech}}$  to balance  $\Delta G \#$  and start martensitic transformation. In other words, the reverse transformation can be triggered if the applied stress is less than this smaller stress.

As is shown in Fig. 1c, chemical free energy change and therefore,  $\Delta G \#$  increases with temperature. As a result, a higher applied stress is required at higher temperature in order to provide a larger  $\Delta G_{\text{mech}}$  for the martensite transformation. When the applied stress is reduced after the onset of the martensite transformation, the reverse transformation can occur at a higher applied stress. On the other hand, at lower temperature,  $\Delta G \#$  can be negative while unloading, which means the specimen still undergoes martensite transformation even  $\Delta G_{\text{mech}} = 0$  (or without applied stress).

The numerical results based on the above discussion are shown in Fig. 11. In these calculations, two particular temperatures are chosen — the equilibrium temper-

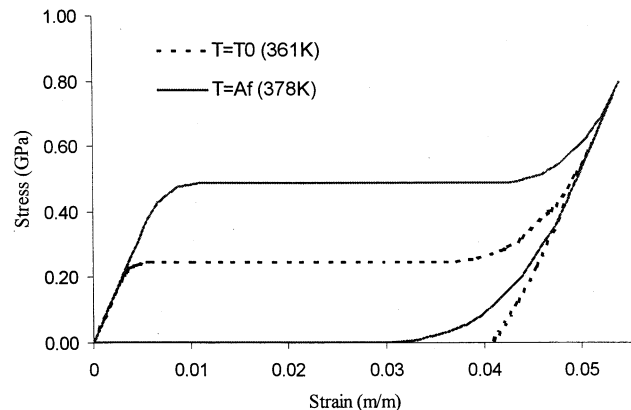


Fig. 11. Temperature effect on loading–unloading curve.

ature  $T_0$  and austenite finish temperature  $A_f$ . At  $T_0$ , the chemical free energy change is equal to zero so that  $\Delta G\#$  is equal to  $-G_f$  while unloading. When the applied stress is reduced to zero, most of the grains remain in martensite structure, i.e. the SMA has a residual strain due to the friction stress. At temperature  $A_f$ ,  $\Delta G\#$  is equal to zero while unloading. A complete strain recovery occurs when the applied stress is removed. This agrees with the phenomenon of SMA at austenite finish temperature.

#### 4. Concluding remarks

A micromechanical model to predict stress–strain behavior for shape memory alloys (SMAs) is presented, where Gibbs free energy minimum condition is employed. As examples, flow curves of TiNiCu SMA single- and poly-crystals are computed and good agreements are obtained between the predictions and experimental data from literature. This model is also applicable to multi-axial stress loading and to a specimen with texture by inputting appropriate loading conditions into  $\sigma_{ij}^0$ .

#### Acknowledgements

The present authors are thankful to National Science Foundation (CMS 9414696) and Defense Advanced Research Agency/Boeing for their supports in conducting this research.

#### Appendix A

Internal stresses within an ellipsoid with  $a = b$ ,  $c/a \rightarrow 0$  subjected by particular eigenstrains.

Internal stresses inside an ellipsoid with  $a = b \gg c$  and with misfit strains are expressed as [21]

$$\begin{aligned} \frac{\sigma_{11}}{2\mu} &= \frac{-v}{1-v}(\varepsilon_{11}^T + \varepsilon_{22}^T) - \varepsilon_{11}^T + \frac{13}{32(1-v)} \frac{\pi c}{a} \varepsilon_{22}^T \\ &\quad + \frac{16v-1}{32(1-v)} \frac{\pi c}{a} \varepsilon_{22}^T - \frac{2v+1}{8(1-v)} \frac{\pi c}{a} \varepsilon_{33}^T \\ \frac{\sigma_{22}}{2\mu} &= \frac{-v}{1-v}(\varepsilon_{11}^T + \varepsilon_{22}^T) - \varepsilon_{22}^T + \frac{16v-1}{32(1-v)} \frac{\pi c}{a} \varepsilon_{11}^T \\ &\quad + \frac{13}{32(1-v)} \frac{\pi c}{a} \varepsilon_{22}^T - \frac{2v+1}{8(1-v)} \frac{\pi c}{a} \varepsilon_{33}^T \\ \frac{\sigma_{33}}{2\mu} &= -\frac{2v+1}{8(1-v)} \frac{\pi c}{a} \varepsilon_{11}^T - \frac{2v+1}{8(1-v)} \frac{\pi c}{a} \varepsilon_{22}^T \\ &\quad - \frac{1}{4(1-v)} \frac{\pi c}{a} \varepsilon_{33}^T \end{aligned}$$

$$\frac{\sigma_{23}}{2\mu} = \frac{v-2}{4(1-v)} \frac{\pi c}{a} \varepsilon_{23}^T \quad (\text{A-1})$$

$$\frac{\sigma_{31}}{2\mu} = \frac{v-2}{4(1-v)} \frac{\pi c}{a} \varepsilon_{31}^T$$

$$\frac{\sigma_{12}}{2\mu} = -\varepsilon_{12}^T + \frac{7-8v}{16(1-v)} \frac{\pi c}{a} \varepsilon_{12}^T$$

If  $c/a \rightarrow 0$ , the internal stresses become:

$$\begin{aligned} \sigma_{11} &= -2\mu \left\{ \frac{v}{1-v}(\varepsilon_{11}^T + \varepsilon_{22}^T) + \varepsilon_{11}^T \right\} \\ \sigma_{22} &= -2\mu \left\{ \frac{v}{1-v}(\varepsilon_{11}^T + \varepsilon_{22}^T) + \varepsilon_{22}^T \right\} \\ \sigma_{12} &= -2\mu \varepsilon_{12}^T \\ \sigma_{33} &= \sigma_{23} = \sigma_{31} = 0 \end{aligned} \quad (\text{A-2})$$

A misfit strains (eigenstrains) given by  $\begin{bmatrix} \varepsilon_{11}^T & 0 & 0 \\ 0 & 0 & 0 \\ 0 & 0 & \varepsilon_{33}^T \end{bmatrix}$

can be transformed to  $\begin{bmatrix} 0 & 0 & \varepsilon_{31}^{T'} \\ 0 & 0 & 0 \\ \varepsilon_{31}^{T'} & 0 & \varepsilon_{33}^{T'} \end{bmatrix}$  by rotation as

discussed in the steps of Eqs. (22)–(24). Then, by using Eq. (A-2) which contains only non-zero components ( $\varepsilon_{11}^T$ ,  $\varepsilon_{22}^T$  and  $\varepsilon_{33}^T$ ) and the  $\varepsilon_{ij}^{T'}$  so transformed, we can prove that all  $\sigma'_{ij} = 0$ .

#### References

- [1] M. Fremond, S. Miyazaki, Shape Memory Alloys, Springer, Wien, New York, 1996, pp. 71, 142.
- [2] M. Taya, A.H.Y. Lue, Y. Tomota, K. Hamada, K. Inoue, A. Shimamoto, Proc. 18th Riso Int. Symp. Mater. Sci. (1997) 191.
- [3] K. Tanaka, F. Nishimura, T. Hayashi, H. Tobushi, C. Lexcelent, Mech. Mater. 19 (1995) 281.
- [4] N. Ono, A. Satoh, Trans. JIM 29 (1988) 267.
- [5] N. Ono, A. Satoh, H. Ohta, Mater. Trans. JIM 30 (1989) 756.
- [6] G.I. Taylor, J. Inst. Met. 62 (1938) 307.
- [7] J.R. Patel, M. Cohen, Acta Met. 1 (1953) 531.
- [8] T.E. Buchheit, J.A. Wert, Met. Trans. A 25A (1994) 2383.
- [9] T.E. Buchheit, S.L. Kumpf, J.A. Wert, Acta Met. 43 (1995) 4189.
- [10] R.J. Comstock Jr, T.E. Buchheit, M. Somerday, J.A. Wert, Acta Met. 44 (1996) 3505.
- [11] E. Patoor, A. Eberhardt, M. Berveiller, Acta Met. 35 (1987) 2779.
- [12] E. Patoor, N. Siredey, A. Eberhardt, M. Berveiller, J. de Physique IV 5 (1995) C8, 227.
- [13] C. Lexcelent, B.C. Goo, Q.P. Sun, J. Bernardini, Acta Met. 44 (1996) 3773.
- [14] J.D. Eshelby, Proc. R. Soc. London A241 (1957) 376.
- [15] T. Saburi, T. Komatsu, S. Nenno, Y. Watanabe, J. Less Common Met. 118 (1986) 217.
- [16] Y. Shugo, H. Hasegawa, T. Honma, Bull. Res. Inst. Mineral Dressing Met. Tohoku Univ. 37 (1981) 79.
- [17] Y.I. Chumlyakov, I.V. Kireeva, V.N. Lineytssev, E.V. Chepel, Y.L. Zuyev, A.I. Lyisyuk, N.S. Surikova, presented at Wayman's memorial symposium, 1996.

- [18] B. Strnadel, S. Ohashi, H. Ohtsuka, T. Ishihara, S. Miyazaki, *Mater. Sci. Eng. A202* (1995) 148.
- [19] H.C. Tong, C.M. Wayman, *Acta Met.* 22 (1974) 887.
- [20] A. Sato, T. Mori, in: C. Youyi, T.Y. Hsu, T. Ko (Eds.), *Proc. Shape Memory alloy'86*, Guilin, China, 1986, p. 353.
- [21] T. Mura, *Micromechanics of Defects in Solids*, second ed., Martinus Nijhoff, Dordrecht, 1987, p. 181.
- [22] T. Mori, K. Tanaka, *Acta Met.* 21 (1973) 571.
- [23] M. Shibata, K. Ono, *Acta Met.* 25 (1977) 35.
- [24] U. Dahmen, K.H. Westmacott, *Acta Met.* 34 (1986) 475.
- [25] M. Kato, T. Fujii, *Acta Met.* 42 (1994) 2929.
- [26] M. Kato, T. Fujii, S. Onaka, *Mater. Sci. Eng. A211* (1996) 95.
- [27] A.A. Griffith, *Phil. Trans. R. Soc. A221* (1920) 163.